

Speeding up Brownian escape via intermediate finite potential barriers

Vishwajeet Kumar,^{1,2} Ohad Shpielberg,³ and Arnab Pal^{1,2, a)}

¹⁾*The Institute of Mathematical Sciences, C.I.T. Campus, Taramani, Chennai 600113, India*

²⁾*Homi Bhabha National Institute, Training School Complex, Anushakti Nagar, Mumbai 400094, India*

³⁾*Haifa Research Center for Theoretical Physics and Astrophysics, University of Haifa, Abba Khoushy Ave 199, Haifa 3498838, Israel*

The mean first-passage time (MFPT) for a Brownian particle to surmount a potential barrier of height ΔU is a fundamental quantity governing a wide array of physical and chemical processes. According to the Arrhenius Law, the MFPT typically grows exponentially with increasing barrier height, reflecting the rarity of thermally activated escape events. In this work, we demonstrate that the MFPT can be significantly reduced by reshaping the original single-barrier potential into a structured energy landscape comprising multiple intermediate barriers of lower heights, while keeping the total barrier height ΔU unchanged. Furthermore, this counterintuitive result holds across both linear and nonlinear potential profiles. Our findings suggest that tailoring the energy landscape—by introducing well-placed intermediate barriers—can serve as an effective control strategy to accelerate thermally activated transitions. These predictions are amenable to experimental validation using optical trapping techniques.

I. INTRODUCTION

Thermally activated escape processes are widespread in science, playing a central role in phenomena such as chemical reactions, protein folding, and nucleation during crystallization. These processes typically involve a system or agent surmounting an energy barrier to transition into a more stable or desired state. In chemical reactions, reactant molecules must overcome an activation barrier to break existing bonds and form new ones, thereby enabling the transformation of reactants into more stable products. In another instance, during protein folding, a polypeptide chain can undergo a series of conformational transitions across multiple intermediate states, by overcoming energy barriers before ultimately attaining its native, stable structure. A key quantity of interest across these scenarios is the average time required to cross the barrier(s). For instance, in chemical reactions, the reaction rate can be estimated as the inverse of this average transition time. In proteins, the folding times characterize the time it takes a protein to attain functional conformation, which is essential for executing its biological activities. Gaining insight into the factors that affect this time, which can be referred as the first-passage time, is thus crucial and a challenging study spanning physics, chemistry, biology and other interdisciplinary studies — see^{1–7} for a review on this topic.

A foundational theoretical framework for understanding barrier-crossing times was established by Kramers in his landmark work⁸. He showed that a Brownian particle attempting to overcome a high potential barrier provides an effective model for calculating reaction rates in chemical processes. To illustrate this, imagine a Brownian particle confined in a metastable state of a potential

landscape $U(x)$, while in contact with a thermal reservoir at temperature T . To escape the trap, the particle must overcome a barrier of height ΔU defined by the potential $U(x)$. The crossing time depends on the interplay between two key forces: the deterministic force arising from the potential $U(x)$, and a stochastic force resulting from thermal fluctuations—random collisions with the bath particles. Kramers showed that in the limit where the barrier height ΔU is much larger than the thermal energy $k_B T$ (with k_B being the Boltzmann constant), the mean escape time \mathcal{T} takes on a well-defined form

$$\mathcal{T} = A e^{\Delta U / k_B T}, \quad (1)$$

where the exponential factor is universal, depending solely on the barrier height ΔU and not on the particular shape of the potential, while the pre-exponential factor A is sensitive to the specific form of the potential and can also depend on the nature of dynamics⁹.

Despite the passage of decades since its inception, Kramers' theory of barrier crossing continues to be a cornerstone in the study of reaction dynamics and remains an active field of research¹⁰. Modern investigations have extended the classical framework into new domains, motivated by developments in nonequilibrium statistical mechanics, complex systems, and active matter. Recent studies have explored a wide range of phenomena: barrier crossing in systems driven by active noise^{11–14}, escape dynamics of composite particles such as dimers^{15–17}, and the influence of long-range temporal correlations or memory effects on the escape time statistics¹⁸. Others have focused on many-body systems where particle interactions play a pivotal role in modifying the escape dynamics^{19–21}.

A prominent theme within this body of work is the search for mechanisms that can *accelerate* the escape process—critical in applications ranging from chemical kinetics to molecular machines. Several innovative strategies have emerged to reduce the mean barrier crossing

^{a)}Electronic mail: arnabpal@imsc.res.in

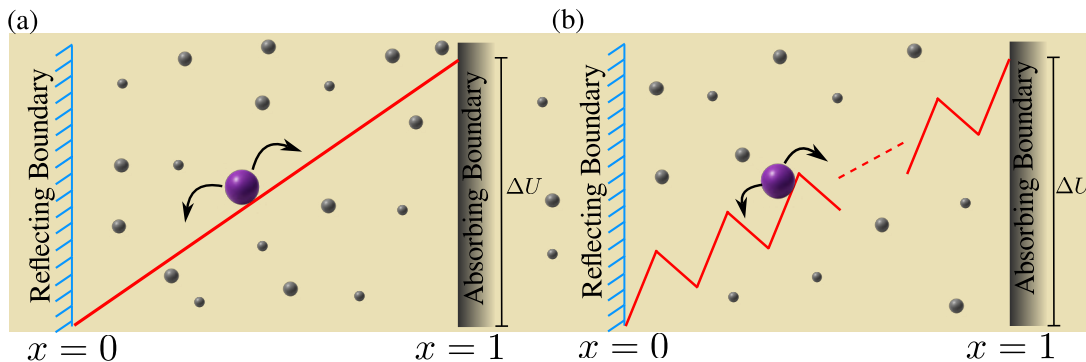


FIG. 1. Panel (a): Schematic of a Brownian particle (large sphere) that starts at $x = 0$, which is a reflecting boundary, and is eventually absorbed at $x = 1$, which is the absorbing boundary, after overcoming a potential barrier of height ΔU . By altering the potential structure by introducing intermediate potential barriers as in panel (b), we would like to examine whether the mean first-passage time to reach the absorbing boundary can be reduced than that from the unaltered potential configuration as in panel (a). The Brownian particle is assumed to be in contact with a thermal bath surrounded by the bath particles (indicated by the smaller spheres).

time. These include: Noise engineering – modulating the memory time of colored noise has been shown to significantly influence the crossing dynamics²²; Stochastic resetting – introducing resetting protocols—where particles are intermittently returned to a specific location—can lead to an optimal escape rate under certain conditions^{23–28}; Time-dependent driving: Applying weak, time-periodic forces to the system can enhance the likelihood of barrier crossing via stochastic resonance mechanisms²⁹. Collectively, these studies signal a paradigm shift in our understanding of thermally activated escape, expanding Kramers’ classical picture into a richer and more diverse landscape of nonequilibrium strategies for controlling barrier crossing times.

Despite significant progress, research on how to manipulate potential landscapes to control the mean barrier crossing time—or equivalently, the mean first-passage time (MFPT)—remains an active and evolving field. This is also important since diffusion of particles, ions, molecules, or even living microorganisms in confined geometries such as tubes and channels plays a key role across various scales in natural and technological processes^{30–32}. One promising direction involves reshaping the potential profile, such as subdividing or optimizing the energy barrier to facilitate more efficient escape^{33–35}. A notable initial contribution in this area is due to Wagner and Kiefhaber³³, who numerically studied the effect of partially folded intermediates along the reaction pathway on the rates of protein folding. By modeling the folding process as the diffusion of reaction coordinates in a potential energy landscape, they showed that placing intermediates within the barrier, without changing its overall height, can enhance folding rates if the intermediate barriers are of moderate heights. Another important contribution in this direction was made by Palyulin and Metzler³⁴, who demonstrated that replacing a simple linear potential with a piecewise linear potential consisting of two segments (while maintaining a fixed barrier

height ΔU) allows for tuning the segment slopes to minimize the MFPT. It was shown that the optimal MFPT achieved in this segmented configuration was lower than that of the original linear potential. Another crucial development along this line was due to Chupeau et al.³⁵, who experimentally demonstrated that the MFPT of the Brownian particle for reaching a target can be reduced by guiding it through a suitably engineered potential barrier profile. This acceleration of the first-passage process was observed in both the underdamped and overdamped regimes.

This naturally leads to the following compelling questions: Can a faster completion be achieved when a potential is composed of multiple segments instead of just two? Can the systematic control of the potential shape—achieved through structural modifications of individual segments—indeed expedite the completion process? The purpose of this work is to study a comprehensive model combined with theory and simulations to address such questions. By leveraging the knowledge of such arrangements, it may become possible to design potential landscapes that serve as regulators of transport, where modifications to the potential shape can systematically control the rate at which large molecules, ions, or metabolites escape through confining channels.

To investigate these questions, we consider a prototypical set-up of a Brownian particle diffusing in a landscape depicted in Fig. 1(a); the particle starts at position $x = 0$, which acts as a reflecting boundary while the boundary at $x = 1$ is absorbing. Let \mathcal{T} denote the mean first-passage time (MFPT) for the particle to reach $x = 1$ by crossing the potential barrier of height ΔU . Now, consider the alternative setup shown in Fig. 1(b), where the potential is replaced with a piecewise structure by introducing multiple intermediate barriers of smaller heights—creating several linear segments—while keeping the overall barrier height ΔU unchanged. We denote the MFPT in this modified potential by \mathcal{T}^{mod} . The central

question we explore is whether a suitably chosen piecewise linear potential can yield a lower MFPT, such that $\mathcal{T}^{\text{mod}} < \mathcal{T}$? Using analytical tools from first-passage theory, we show that by carefully tuning the slopes of the individual segments in the piecewise linear potential, the MFPT can be significantly reduced. Moreover, we find that increasing the number of intermediate barriers—i.e., the number of adjustable segments—further decreases the MFPT, yielding a powerful control for optimizing escape times. These insights are not limited to linear potentials. We extend our analysis to non-linear landscapes as well, demonstrating that analogous improvements in MFPT can be achieved by replacing smooth non-linear potentials with carefully constructed piecewise non-linear profiles, as illustrated in Fig. 4(b). These general findings establish the introduction of intermediate barriers as a general and robust technique for facilitating faster barrier crossing in diffusive systems.

The paper is organized in the following way. The system set up is described in section II. This section further discusses the first-passage formalism to compute the MFPT. In section III A, we review the case of single barrier³⁴ and extend to other potentials in section III B. Section (IV) discusses the impact of introducing multiple intermediate barriers in both linear and non-linear potential landscapes. It is shown that a systematic arrangement of barriers can lead to a successive reduction in the MFPT with increasing number of barriers employed. We conclude in Sec. V with a future outlook. Some additional details are included to the appendices.

II. SETUP AND REVIEW OF THE FIRST-PASSAGE FORMALISM

Consider a Brownian particle, whose position $x(t)$ is described by the overdamped Langevin equation in an external potential $U(x)$ ^{36,37}

$$\dot{x}(t) = -\frac{U'(x)}{\gamma} + \sqrt{2D}\eta(t), \quad (2)$$

where $\eta(t)$ is a Gaussian white noise with the following statistical properties

$$\langle \eta(t) \rangle = 0, \quad \langle \eta(t)\eta(t') \rangle = \delta(t - t'). \quad (3)$$

By the fluctuation dissipation theorem, $D = k_B T / \gamma$, where γ is the viscosity of the surrounding medium, which we assume to be unity, implying $D = k_B T$. We confine the particle in the region $x \in [0, 1]$ as shown in Fig. 1(a). The particle starts from $x_0 \in [0, 1]$ and it must surmount a potential barrier of height $\Delta U = U(x = 1) - U(x = 0)$, in order to be absorbed at $x = 1$. Furthermore, without loss of generality, we set $U(x = 0) = 0$ which implies that $U(x = 1) = \Delta U$.

In this specific set up, the MFPT, $\mathcal{T}(x_0)$, is the average time it takes for the particle to get absorbed at $x = 1$ starting from an initial position $x_0 \in [0, 1]$. To find

$\mathcal{T}(x_0)$, we start by writing the backward Fokker Planck equation, for the survival probability $\mathcal{P}(t, x_0)$, which denotes the probability that the particle has not been absorbed up to time t , given that it started at position x_0 at $t = 0$. From $\mathcal{P}(t, x_0)$, the first-passage time density is derived using

$$\mathcal{F}(t, x_0) = -\frac{\partial}{\partial t} \mathcal{P}(t, x_0), \quad (4)$$

where $\mathcal{F}(t, x_0)dt$ represents the probability that the particle has been absorbed in the time between t and $t + dt$. The MFPT is then obtained using the following relation

$$\mathcal{T}(x_0) = \int_0^\infty t \mathcal{F}(t, x_0) dt, \quad (5)$$

which satisfies the following backward Fokker-Planck equation⁹:

$$-U'(x_0) \frac{\partial}{\partial x_0} \mathcal{T}(x_0) + k_B T \frac{\partial^2}{\partial x_0^2} \mathcal{T}(x_0) = -1, \quad (6)$$

where note that the initial position x_0 is now being treated as a variable⁹. To determine $\mathcal{T}(x_0)$, this equation must be solved subject to the two boundary conditions

$$\left. \frac{\partial}{\partial x_0} \mathcal{T}(x_0) \right|_{x_0=0} = 0, \quad \text{and} \quad \mathcal{T}(x_0 = 1) = 0. \quad (7)$$

To compute the corresponding MFPT for an arbitrary potential, sometimes it is useful to recast Eq.(6) into an integral form⁹

$$\mathcal{T}(x_0) = \frac{1}{k_B T} \int_{x_0}^1 dx'' e^{U(x'')/k_B T} \int_0^{x''} dx' e^{-U(x')/k_B T}, \quad (8)$$

where we have already imposed the boundary conditions. Setting $x_0 = 0$, we will henceforth denote the MFPT as \mathcal{T} . Moreover, we will also adopt the following notation: U_N^L refers to a potential with N barriers/kinks, where each segment is linear. The associated MFPT for this potential is denoted by \mathcal{T}_N^L . Similarly, U_N^H represents a potential with N barriers/kinks, where each segment is harmonic. The corresponding MFPT for this potential is denoted by \mathcal{T}_N^H .

III. INTRODUCING ONE INTERMEDIATE BARRIER

In this section, we demonstrate that introducing an intermediate barrier (or kink) in potential landscapes and adjusting the strength of the segments on either side of the kink, while keeping the kink position and overall barrier height fixed, can reduce the MFPT compared to the original potential profile.

In Section III A, we briefly reproduce the results of Palyulin and Metzler³⁴ for the case of a linear potential. In Section III B, we extend it to consider a harmonic potential, investigating whether such modification results in a reduction of the MFPT in this case as well.

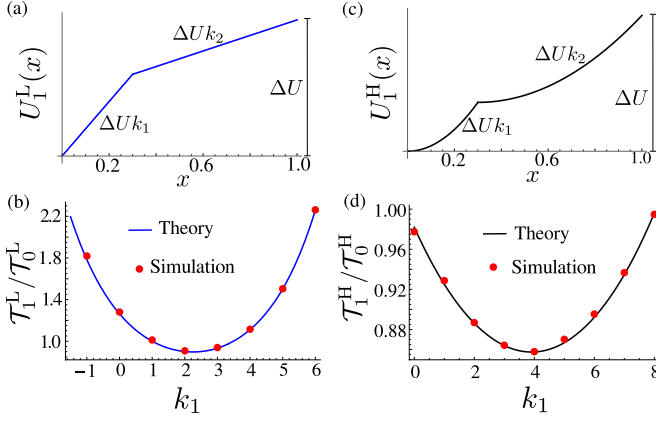


FIG. 2. Panels (a) & (c): Piecewise linear and harmonic potential with a single kink at $x = a = 0.3$. Panel (b): The inverse speed up factor, $\mathcal{T}_1^L/\mathcal{T}_0^L$, for linear case is plotted as a function of k_1 with $\Delta U = 3$ and $a = 0.3$. For a range of k_1 values, $\mathcal{T}_1^L/\mathcal{T}_0^L$ is less than 1, implying that the modification has accelerated the process completion in these regimes. Panel (d): The inverse speed-up factor, $\mathcal{T}_1^H/\mathcal{T}_0^H$, for harmonic case is plotted as a function of k_1 for $\Delta U = 3$ and $a = 0.3$. Similar to the linear case, $\mathcal{T}_1^H/\mathcal{T}_0^H < 1$ for several k_1 values. Simulation data are shown as points, and the analytical solution is plotted as continuous curve and $k_B T$ is taken to be 1.

A. MFPT reduction in linear potential

Consider a linear potential described as follows:

$$\frac{U_0^L(x)}{\Delta U} = x, \quad 0 \leq x \leq 1 \quad (9)$$

To determine the MFPT associated with this potential, we solve Eq.(6) subject to the two boundary conditions in Eq.(7). This leads to the following expression for the MFPT for the particle starting at $x_0 = 0$:

$$\mathcal{T}_0^L = \frac{1}{\Delta U^2} (k_B T e^{\Delta U/k_B T} - \Delta U - k_B T). \quad (10)$$

We now modify the linear potential into a piecewise-linear form consisting of two segments, defined as:

$$\frac{U_1^L(x)}{\Delta U} = \begin{cases} k_1 x, & 0 \leq x \leq a \\ k_2(x - a) + k_1 a, & a \leq x \leq 1 \end{cases} \quad (11)$$

where, k_1 and k_2 can be thought of as the strength of the potential segments which can take any real values. Imposing the setup constraint $U_1^L(x = 1) = \Delta U$ implies

$$\Delta U = \Delta U[k_1 a + k_2(1 - a)] \quad (12)$$

Fig.2(a) depicts this potential (Eq.(9)) for one particular values of k_1 , k_2 and a . To determine the associated MFPT, we solve Eq. (6) separately over two regions: Region I, defined on the interval $x_0 \in [0, a]$, and Region II, defined on $x_0 \in [a, 1]$. The general solutions in each region contain constants of integration, which are

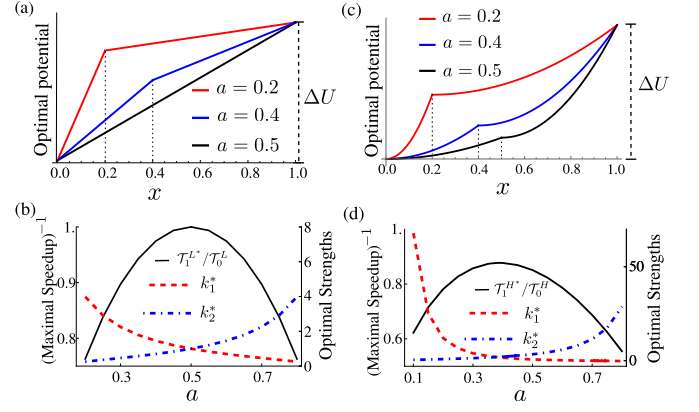


FIG. 3. Panels (a) & (c) show the optimal potential profiles (for various values of a) for the case of one kink in linear and harmonic potentials respectively. Panel (b) shows the variation of the inverse maximal speed-up factor and the corresponding optimal strengths with a , for the linear case, with $\Delta U = 3$. The left vertical axis represents this dimensionless factor, while the right vertical axis indicates the corresponding optimal strengths, k_1^* and k_2^* . For $a = 0.5$, we observe $k_1^* = k_2^*$, implying that the optimal potential is the original linear potential itself in this case from panel (a). Panel (d) depicts the variation of these quantities for harmonic case, for $\Delta U = 3$. It shows that the inverse maximal speed-up factor never reaches unity. Similar to the linear case, there exists a range of a values for which $k_1^* > k_2^*$, while for other values, $k_2^* > k_1^*$ as shown in panel (d). The MFPTs are determined analytically and the corresponding optimal values have been found numerically, while fixing $k_B T$ to unity.

determined by enforcing the two boundary conditions, together with the following matching conditions at the position of the kink (see Appendix A for details)

$$\mathcal{T}_{1,I}^L(x_0 = a) = \mathcal{T}_{1,II}^L(x_0 = a) \quad (13)$$

and

$$\partial_{x_0} \mathcal{T}_{1,I}^L(x_0 = a) = \partial_{x_0} \mathcal{T}_{1,II}^L(x_0 = a) \quad (14)$$

where, $\mathcal{T}_{1,I}^L(x_0)$ (or $\mathcal{T}_{1,II}^L(x_0)$) denotes the MFPT if the particle starts in region I (or II). Applying these conditions determines the MFPT as a function of x_0 . For $x_0 = 0$, it takes the following form

$$\begin{aligned} \mathcal{T}_1^L = & -\frac{k_B T}{\Delta U^2} \left(\frac{1}{k_1^2} + \frac{1}{k_2^2} \right) - \frac{a}{k_1 \Delta U} - \frac{1-a}{k_2 \Delta U} + \frac{k_B T}{k_1 k_2 \Delta U^2} \\ & + \frac{k_B T}{\Delta U^2} \left(\frac{1}{k_1^2} - \frac{1}{k_1 k_2} \right) e^{a k_1 \Delta U / k_B T} + \frac{k_B T}{k_1 k_2 \Delta U^2} e^{\Delta U / k_B T} \\ & + \frac{k_B T}{\Delta U^2} \left(\frac{1}{k_2^2} - \frac{1}{k_1 k_2} \right) e^{k_2(1-a) \Delta U / k_B T} \end{aligned} \quad (15)$$

At fixed values of a and ΔU , MFPT only depends on k_1 and k_2 . However, due to the constraint in Eq.(12), only one of k_1 and k_2 is free. We take k_1 to be the free parameter so that k_2 is automatically determined by

$k_2 = (1 - k_1 a)/(1 - a)$. In Fig.2(b), we plot $\mathcal{T}_1^L/\mathcal{T}_0^L$ as a function of k_1 for fixed $a = 0.3$. Quite interestingly, for a range of k_1 values, this ratio remains below unity, implying that the modification leads to a reduction in the MFPT compared to the unmodified case in this parameter regime. This reduction can be attributed to the interplay of the times taken in traversing the two segments of the modified linear potential³⁴. By tuning the strengths k_1 and k_2 , the additional time required to cross the steeper segment—relative to crossing the same spatial portion of unmodified potential with strength ΔU —can be outweighed by the time gained on the shallower segment. For appropriate choices of k_1 and k_2 , this trade-off leads to a net decrease in the MFPT compared to the unmodified case. To quantify this, we introduce the factor speed-up which will be discussed next.

Maximal speedup for the process completion: We define the speedup factor as the ratio of the MFPT corresponding to the original unmodified potential to that corresponding to the potential modified by the introduction of intermediate barrier(s). In the present case, it is given by $\mathcal{T}_0^L/\mathcal{T}_1^L$. A ratio less than unity indicates that the modification results in slowing down the process, whereas a ratio greater than unity signifies the acceleration of the process. In Fig.2(b), we plot the inverse of this factor with k_1 for a given a , which shows that for a range of k_1 values, the inverse speedup factor $\mathcal{T}_1^L/\mathcal{T}_0^L < 1$, implying that in this range the first passage process is accelerated by the modified potential, as compared to the unmodified one.

Further, as k_1 is varied, the inverse speed-up factor $\mathcal{T}_1^L/\mathcal{T}_0^L$ exhibits a minimum at a specific value, denoted by k_1^* . We denote this minimum MFPT by $\mathcal{T}_1^{L*} = \mathcal{T}_1^L|_{k_1=k_1^*}$, so that the speed-up ratio $\mathcal{T}_0^L/\mathcal{T}_1^{L*}$ is maximum. The inverse maximal speedup factor is plotted as a function of a in Fig.3(b). For $a < 1/2$, the optimal strengths satisfy $k_1^* > k_2^*$, whereas for $a > 1/2$, $k_1^* < k_2^*$, indicating that in the optimal configuration, the region with the steeper strength occupies the smaller fraction of the spatial domain. Interestingly, $\mathcal{T}_1^{L*}/\mathcal{T}_0^L \leq 1$, with equality only at $a = 1/2$. This implies that the minimum MFPT is strictly smaller than the MFPT of the unmodified linear potential, or in other words, the maximal speed-up ratio is greater than 1 for all $a \neq 1/2$. At $a = 1/2$, the equality $\mathcal{T}_1^{L*} = \mathcal{T}_0^L$ arises because the optimal strengths satisfy $k_1^* = k_2^*$ (see Fig. 3(b)), indicating that the optimal potential coincides with the original linear potential. These observations demonstrate that introducing an intermediate barrier into a linear potential enables a robust reduction in MFPT and therefore a robust speeding-up of the process completion across the entire range of a .

B. MFPT reduction in harmonic potential

We now turn our attention to the motion in the presence of a harmonic potential described by

$$\frac{U_0^H(x)}{\Delta U} = x^2, \quad 0 \leq x \leq 1. \quad (16)$$

The corresponding MFPT for the particle, starting at $x_0 = 0$, can be obtained by solving Eq.(6) with the two boundary conditions, and reads

$$\mathcal{T}_0^H = \frac{1}{2k_B T} {}_2F_2\left(1, 1; \frac{3}{2}, 2; \frac{\Delta U}{k_B T}\right) \quad (17)$$

where ${}_pF_q(a_1, \dots, a_p; b_1, \dots, b_q; z)$ stands for the generalized hypergeometric function. We now introduce a kink in the harmonic potential at $x = a$ (see Fig.2(c)) defining a piecewise harmonic potential as follows

$$\frac{U_1^H(x)}{\Delta U} = \begin{cases} k_1 x^2, & 0 \leq x \leq a \\ k_2(x-a)^2 + k_1 a^2 & a \leq x \leq 1 \end{cases} \quad (18)$$

where, k_1 and k_2 denote the strength of the potential segments which can take any real value. The set up constraint naturally implies

$$U_1^H(x=1) = \Delta U = \Delta U[k_1 a^2 + k_2(1-a)^2]. \quad (19)$$

The associated MFPT for this modified potential is derived following Section III A, yielding

$$\begin{aligned} \mathcal{T}_1^H = & \frac{e^{\frac{a^2 k_1 \Delta U}{k_B T}} \pi \operatorname{erf}\left(\frac{a\sqrt{k_1 \Delta U}}{\sqrt{k_B T}}\right) \operatorname{erfi}\left(\frac{(1-a)\sqrt{k_2 \Delta U}}{\sqrt{k_B T}}\right)}{4\sqrt{k_1 k_2} \Delta U} \\ & - \frac{\pi \operatorname{erf}\left(\frac{(1-a)\sqrt{k_2 \Delta U}}{\sqrt{k_B T}}\right) \operatorname{erfi}\left(\frac{(-1+a)\sqrt{k_2 \Delta U}}{\sqrt{k_B T}}\right)}{4k_2 \Delta U} \\ & + \frac{a^2}{2k_B T} {}_2F_2\left(1, 1; \frac{3}{2}, 2; \frac{a^2 k_1 \Delta U}{k_B T}\right) \\ & - \frac{(-1+a)^2}{2k_B T} {}_2F_2\left(1, 1; \frac{3}{2}, 2; -\beta\right), \end{aligned} \quad (20)$$

where $\beta = (1-a)^2 k_2 \Delta U / k_B T$ and $\operatorname{erf}(z) = \frac{2}{\sqrt{\pi}} \int_0^z e^{-y^2} dy$ denotes the error function, $\operatorname{erfi}(z) = -i \operatorname{erf}(iz)$ denotes the imaginary error function. Following a similar approach as in Section III A, we obtain Fig.2(d), which illustrates the dependence of the inverse speed-up factor, $\mathcal{T}_1^H/\mathcal{T}_0^H$, on k_1 for the harmonic case. As in the linear case, $\mathcal{T}_1^H/\mathcal{T}_0^H < 1$ over a range of k_1 , indicating a reduced MFPT for the modified potential compared to the unmodified harmonic case.

Maximal speedup for the process completion: Likewise the piecewise linear potential, the inverse speed-up factor exhibits a minimum as shown in Fig.2(d), which corresponds to the maximal speedup of the process completion. Further, Fig.3(d) presents the variation of the

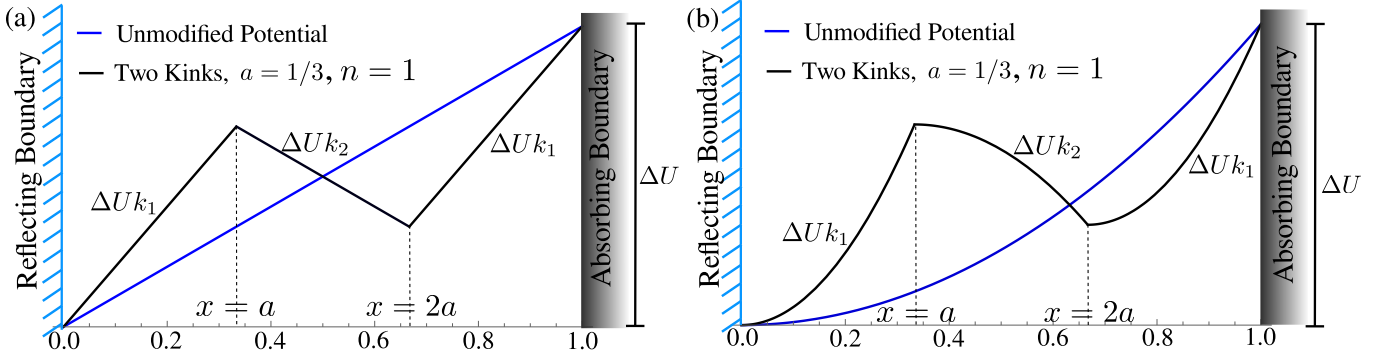


FIG. 4. The figure presents the linear and harmonic potentials (in blue) along with their corresponding modified potentials after introducing $N = 2n = 2$ kinks (in black), as shown in panels (a) and (b), respectively. The modified potential consists of segments with alternating strengths k_1 and k_2 . In both cases, the kinks are equally spaced and positioned at $x = a$ and $x = 2a$, where $a = 1/3$.

inverse maximal speed-up factor, $\mathcal{T}_1^{\text{H}^*}/\mathcal{T}_0^{\text{H}}$, and optimal strengths k_1^* and k_2^* with a , where k_1^* (and k_2^*) for a given a corresponds to the minimum MFPT and therefore the maximal speedup in the process completion for that specific value of a . See Fig.3(c) for a few representative optimal potential profiles. Further, Fig.3(d) shows that there exists a range of the parameter a such that $k_1^* > k_2^*$, and at other values, $k_2^* > k_1^*$. Interestingly, we find $\mathcal{T}_1^{\text{H}^*}/\mathcal{T}_0^{\text{H}} < 1$ for all a , demonstrating a robust reduction in the optimal MFPT across the entire range of a , thus showcasing a similar optimization.

IV. INTRODUCING MULTIPLE INTERMEDIATE BARRIERS

Previously, we analyzed the effect of incorporating a single intermediate barrier on the controlled reduction of the mean first-passage time (MFPT). The aim of this section is to extend this analysis by introducing multiple intermediate barriers in the potential structure. As a means to achieve this, the potential is restructured into segments with alternating strengths of k_1 and k_2 , starting with k_1 ; an illustration for a three-segment case is provided in Fig. 4. This introduces intermediate barriers, with their number N equal to one less than the number of segments, $N + 1$. For simplicity, we assume the kinks are uniformly spaced in the interval $x \in [0, 1]$, located at $x = a, 2a, \dots, Na$ with $a = 1/(N + 1)$, where N is the number of kinks.

A. Observation I: Intermediate barriers resulting from even number of segmentations do not facilitate the further reduction of the MFPT with increasing segments

Let us consider the linear potential as in Eq.(9), partitioned now into $N + 1$ segments by introducing N kinks, where N is assumed to be odd. The potential then consists of $(N + 1)/2$ segments each with strengths

k_1 and k_2 . Under this condition, the set up constraint, $U_N^{\text{L}}(x = 1) = \Delta U$, implies:

$$U_N^{\text{L}}(x = 1) = \Delta U = \Delta U \frac{N+1}{2} k_1 a + \Delta U \frac{N+1}{2} k_2 a \quad (21)$$

We analytically solve Eq.(6) to compute the MFPT, \mathcal{T}_N^{L} , using mathematica. This computation involves the two boundary conditions and $2N$ connecting conditions, two per kink (see Appendix A for the details). Following the method in Section III, we determine the minimum MFPT, $\mathcal{T}_N^{\text{L}*}$, for various odd values of N and compute the inverse maximal speed-up factor, $\mathcal{T}_N^{\text{L}*}/\mathcal{T}_0^{\text{L}}$. Fig.5(a) shows its variation along with the corresponding optimal strengths k_1^* and k_2^* as a function of odd N . The result $\mathcal{T}_N^{\text{L}*}/\mathcal{T}_0^{\text{L}} = 1$ for all odd N shows that introducing such intermediate barriers does not reduce the MFPT in the linear case.

We now analyse the case of harmonic potential. Similar to the case of linear potential, the constraint for $N + 1$ harmonic segments (N odd) is

$$U_N^{\text{H}}(x = 1) = \Delta U = \Delta U \frac{N+1}{2} k_1 a^2 + \Delta U \frac{N+1}{2} k_2 a^2 \quad (22)$$

Following the same procedure as for the linear case, we compute the inverse maximal speed-up factor, $\mathcal{T}_N^{\text{H}*}/\mathcal{T}_0^{\text{H}}$, and the corresponding optimal strengths k_1^* and k_2^* . Figure 6(a) shows their dependence on odd N . While the modified harmonic potential yields a lower MFPT than the unmodified case, the minimal MFPT increases with N , indicating that the maximum reduction occurs at $N = 1$. Thus, adding more kinks does not further accelerate the absorption.

B. Observation II: Intermediate barriers resulting from odd number of segmentations of potential landscapes do facilitate the successive reduction of the MFPT

Let us now modify the linear potential as in Eq.(9) by dividing it into three segments (two kinks) as shown

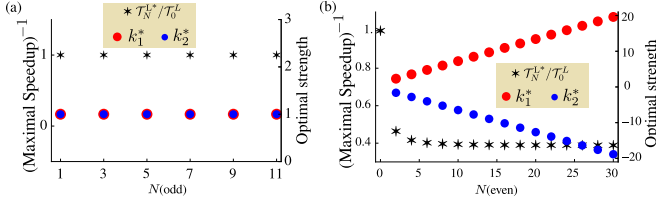


FIG. 5. Variation of the inverse maximal speed-up factor, $\mathcal{T}_N^L/\mathcal{T}_0^L$, and the optimal strengths, with the number of kinks N . The left vertical axis represents the inverse maximal speed-up factor, while the right vertical axis corresponds to optimal strengths, k_1^* and k_2^* . The barrier height is fixed at $\Delta U = 5$ and $k_B T = 1$. To obtain these results, the MFPT for a given N is first computed analytically using Mathematica and the corresponding optimal MFPT is evaluated by numerical minimization. Panel (a) shows that for any odd N , the inverse maximal speed-up factor is unity, indicating no reduction in the MFPT. In these cases, the optimal strengths satisfy $k_1^* = k_2^*$. Panel (b) illustrates the behavior for even values of $N = 2n$. The inverse maximal speed-up factor is less than 1 and decreases monotonically, indicating successive reduction of the MFPT with increasing N . The case $N = 0$ corresponds to the unmodified linear potential.

in Fig. 4(a). The resulting piecewise-linear potential is given by

$$\frac{U_2^L(x)}{\Delta U} = \begin{cases} k_1 x & 0 \leq x \leq a \\ k_2(x - a) + k_1 a & a \leq x \leq 2a \\ k_1(x - 2a) + (k_1 + k_2)a & 2a \leq x \leq 1 \end{cases} \quad (23)$$

Here, the kinks are located at $x = a$ and $x = 2a$, with $a = 1/3$. Imposing the constraint $U_2^L(x = 1) = \Delta U$ yields $\Delta U = \Delta U[2k_1 + k_2]a$. Generalizing to N kinks (with even N), the potential is divided into $N + 1$ segments. Letting $n = N/2$, the condition $U_N^L(x = 1) = \Delta U$ gives:

$$\Delta U = \Delta U(n + 1)k_1 a + \Delta U n k_2 a \quad (24)$$

The inverse maximal speed-up factor, $\mathcal{T}_N^L/\mathcal{T}_0^L$, along with the corresponding optimal strengths k_1^* and k_2^* for various even values of N , is computed following the procedure outlined in Section IV A. As shown in Fig. 5(b), the inverse maximal speed-up factor decreases with increasing N , satisfying $\mathcal{T}_N^L/\mathcal{T}_0^L < 1$ for all $N > 0$ (with $N = 0$ corresponding to the unmodified linear potential). This monotonic decrease indicates that adding more such intermediate barriers is beneficial.

We now analyze the case of harmonic potential. As an example, consider partitioning the harmonic potential in Eq. (16) into three segments, by introducing two kinks. The resulting piecewise-harmonic potential is given by

$$\frac{U_2^H(x)}{\Delta U} = \begin{cases} k_1 x^2 & 0 \leq x \leq a \\ k_2(x - a)^2 + k_1 a^2 & a \leq x \leq 2a \\ k_1(x - 2a)^2 + (k_1 + k_2)a^2 & 2a \leq x \leq 1 \end{cases} \quad (25)$$

See Fig. 4(b) for a schematic of this potential. Imposing $U_2^H(x = 1) = \Delta U$ implies $\Delta U = \Delta U(2k_1 + k_2)a^2$. For

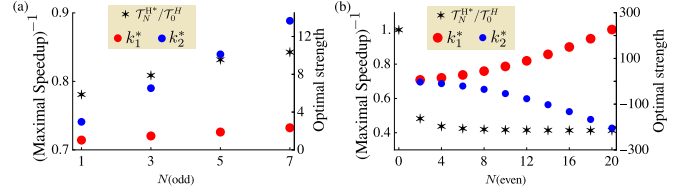


FIG. 6. Variation of the inverse maximal speed-up factor, $\mathcal{T}_N^H/\mathcal{T}_0^H$, and the optimal strengths with N . The barrier height is fixed at $\Delta U = 5$ and $k_B T = 1$. Panel (a): For odd N , the inverse speed-up factor is less than one, indicating reduced MFPT as compared to that for unmodified potential. However, additional kinks doesn't lead to further reduction. Panel (b) illustrates the behavior for even values of $N = 2n$, where the introduction of kinks leads to a reduction in the optimal MFPT. Moreover, the minimal MFPT decreases monotonically with increasing N , indicating that the introduction of additional kinks further reduces the MFPT. The case $N = 0$ corresponds to the unmodified linear potential.

any N (even) number of kinks, the constraint becomes

$$U_N^H(x = 1) = \Delta U = \Delta U(n + 1)k_1 a^2 + \Delta U n k_2 a^2 \quad (26)$$

where, $n = N/2$. A similar analysis to that for the linear case reveals that the inverse maximal speed-up factor, $\mathcal{T}_N^H/\mathcal{T}_0^H$, decreases monotonically with increasing number of such intermediate barriers, or equivalently, with increasing even N (see Fig. 6(b)). The figure also shows the variation of k_1^* and k_2^* with N .

We have thus demonstrated that the the minimum MFPT decreases monotonically with increasing even values of N in both the linear and harmonic cases. This monotonic decrease implies that the maximal speedup achievable in the completion time of the process increases with increasing even N , i.e., $\mathcal{T}_0^L/\mathcal{T}_N^L < \mathcal{T}_0^L/\mathcal{T}_{N+2}^L$ (similarly $\mathcal{T}_0^H/\mathcal{T}_N^H < \mathcal{T}_0^H/\mathcal{T}_{N+2}^H$ for the harmonic case) for all even N . This behavior is attributed to “additional degrees of freedom” which emanates from the incorporation of more kinks/barriers into the potential profile. Each pair of additional kinks (i.e., increasing N to $N + 2$) seems to introduce greater control in shaping the potential profile as the enhanced degree redistributes the strengths of the uphill and downhill segments in a manner that reduces the overall traversal time, resulting in $\mathcal{T}_{N+2}^L < \mathcal{T}_N^L$ (and $\mathcal{T}_{N+2}^H < \mathcal{T}_N^H$).

We continue to investigate the behavior of the optimal potential profiles in the large and even $N \rightarrow \infty$ limit. To this end, we plotted the optimal profiles for large N ($= 30$) in Fig. 7, which is helpful in understanding the asymptotic structure. To determine the scaling of the optimal strength k_1^* , we fitted the dataset $\{k_1^*, N\}$ for even values of N from $N = 2$ to $N = 20$, and confirmed that it correctly gives the result at larger values of N (up to $N = 100$). For $\Delta U = 5$, the resulting fit for the linear case is

$$k_1^* \approx 1.058 + 0.618 N, \quad (27)$$

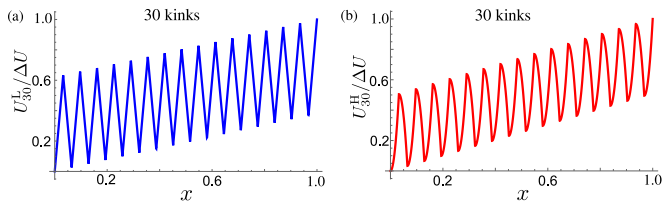


FIG. 7. Panels (a) & (b): Optimally restructured potential configurations in linear and harmonic case for $N = 30$, $\Delta U = 5$ and $k_B T = 1$.

while for the harmonic case it is

$$k_1^* \approx 1.185 + 1.505 N + 0.487 N^2, \quad (28)$$

where the symbol \approx indicates that the coefficients have been rounded to three decimal places. Once k_1^* is known, the corresponding value of k_2^* can be computed using the constraint equations, Eq. (24) for the linear case and Eq. (26) for the harmonic case.

V. CONCLUSIONS AND DISCUSSION

In this work, we investigate how the mean first-passage time (MFPT) of a Brownian particle can be controlled by tailoring the shape of the external potential. We show that the MFPT required for a particle to cross a potential barrier of height ΔU can be markedly reduced by systematically modifying the potential landscape, without altering the overall barrier height. In particular, we demonstrate that replacing a single large barrier with a sequence of smaller intermediate barriers—constructed by partitioning the landscape into segments via the introduction of kinks—leads to a significant acceleration of the first-passage process.

These observations were based on rigorous analysis of the MFPT in a linear and harmonic potential, both unperturbed and modified likewise. We began our analysis by demonstrating that the introduction of a single intermediate barrier in the potential can result in the reduction of the MFPT compared to that of the original unmodified potential. Building on this, we extended the study to the case of multiple equidistant kinks, denoted by N , and investigated the corresponding effects on the MFPT. We further examined a speed-up factor to quantitatively account for the efficacy of the transition rendered by the intermediate barriers. The results are summarized in Table I.

This study has demonstrated that modifying the potential landscape can be an effective strategy for reducing the mean first-passage time (MFPT) of an overdamped Brownian particle. In particular, the piecewise harmonic potential offers a realistic and experimentally accessible model. It can be readily implemented using arrays of optical traps^{38–40}, making it a practical framework for experimentalists and a promising tool for exploring such mechanisms in real systems. This work also points out to

several important directions that remain open. Although our findings suggest that introducing intermediate barriers into complex potential landscapes generally lowers the MFPT, a rigorous theoretical proof of this observation is certainly lacking. Establishing such a result or identifying the extent to which these controls are robust would be a crucial step forward, with potential implications for processes such as molecular or ionic transport through membranes and channels^{32,41}. Another promising direction is to explore the optimal number of subdivisions in complex potential landscapes, extending similar ideas as in⁴², where the potential was partitioned into linear segments within a specific setup which preserves the area under the potential. Unlike our current work that achieves MFPT reduction by tuning the strengths of the potential segments, this optimization with regard to the number of barriers could be another prospecting robust control over the barrier crossing time. In addition, it would be worthwhile to investigate whether similar reductions in first-passage times can be achieved for inertial, underdamped Brownian particles through analogous modifications of the potential.

VI. ACKNOWLEDGMENT

The numerical calculations reported in this work were carried out on the Kamet cluster, which is maintained and supported by the Institute of Mathematical Science's High-Performance Computing Center. VK and AP gratefully acknowledge research support from the Department of Atomic Energy, Government of India via the Apex Projects. AP acknowledges the support from the International Research Project (IRP) titled “Classical and quantum dynamics in out of equilibrium systems” by CNRS, France. OS and AP thank the Korea Institute for advanced Study (KIAS), Seoul, for hospitality during the conference “Nonequilibrium Statistical Physics of Complex Systems” where several discussions related to the project took place.

Appendix A: Discussions on Connecting Conditions and MFPT Computation in the Presence of Intermediate Barriers in Linear and Harmonic Potentials

The aim of this appendix is to derive the matching conditions, for the case when a potential has a single and multiple kinks in it. Although such conditions are natural and can generically be found in textbooks such as^{9,37}, we provide this discussion for completeness. Consider a generic potential $U(x_0)$ which has a kink at $x_0 = a$. Therefore, $U'(x_0)$ is finitely discontinuous and $U''(x_0)$ is infinitely discontinuities at $x_0 = a$. For such potentials, these discontinuities appear in the left hand side (LHS) of the differential equation, Eq.(6). However, the right hand side (RHS) of Eq.(6) is identically equal to -1 and hence remains continuous, regardless of the form of the

TABLE I. Summary of main results. We recall that \mathcal{T}_N^L denotes the MFPT for a piecewise linear potential with $N + 1$ segments or N kinks. The case $N = 0$ refers to the pure linear potential. The MFPT for the piecewise Harmonic potential with N kinks is \mathcal{T}_N^H , where again, the case of $N = 0$ refers to the pure Harmonic potential.

Potential Type	# of kinks (N)	Optimal Shape	MFPT Behavior with N
Piecewise Linear	Even	Non-uniform segment strengths	$\mathcal{T}_N^{L*} < \mathcal{T}_0^L$ and \mathcal{T}_N^{L*} monotonically decreases with N
	Odd	Uniform linear potential	Linear case always optimal
Piecewise Harmonic	Even	Non-uniform segment strengths	$\mathcal{T}_N^{H*} < \mathcal{T}_0^H$ and \mathcal{T}_N^{H*} monotonically decreases with N
	Odd	Non-uniform segment strengths	$\mathcal{T}_N^{H*} < \mathcal{T}_0^H$ for some N , but \mathcal{T}_N^{H*} increases with N

potential $U(x_0)$ on the LHS. It follows that the discontinuities on the LHS must cancel in such a way that the LHS becomes continuous, consistent with the continuity of the RHS.

There are two potential scenarios for the cancellation of this discontinuity

1. $\mathcal{T}'(x_0)$ is finitely discontinuous at $x_0 = a$ resulting in $\mathcal{T}''(x_0)$ being infinitely discontinuous there.
2. $\mathcal{T}'(x_0)$ is continuous at $x_0 = a$ while $\mathcal{T}''(x_0)$ is finitely discontinuous at that point.

The first possibility is rejected as an infinite discontinuity cannot cancel out a finite discontinuity. Therefore, we are left only with the second option. This implies that $\mathcal{T}''(x_0)$ must be finitely discontinuous at $x_0 = a$, which can get cancelled by the finite discontinuity of $U'(x_0)$ at $x_0 = a$. It therefore follows that $\mathcal{T}'(x_0)$ must remain continuous at $x_0 = a$. This automatically implies that $\mathcal{T}(x_0)$ must also be continuous at this point. Thus, we have found the two connecting conditions : $\mathcal{T}(x_0)$ and $\mathcal{T}'(x_0)$ must be continuous at $x_0 = a$.

Note that the two connecting conditions can also be derived as follows. First, we recast Eq.(6) into the following form

$$k_B T \frac{d}{dx_0} \left[e^{-U(x_0)/k_B T} \frac{d}{dx_0} \mathcal{T}(x_0) \right] = -e^{-U(x_0)/k_B T}. \quad (\text{A1})$$

Since a is the position of the kink, we integrate Eq.(A1) from $a - \epsilon$ to $a + \epsilon$, where ϵ is a small positive number. The right-hand side becomes zero because $e^{-U(x_0)/k_B T}$ is a continuous function, as $U(x_0)$ is continuous. Therefore, we obtain:

$$e^{-U(x_0)/k_B T} \frac{d}{dx_0} \mathcal{T}(x_0) \Big|_{x_0=a-\epsilon}^{x_0=a+\epsilon} = 0. \quad (\text{A2})$$

Since $e^{-U(x_0)/k_B T}$ is continuous at $x_0 = a$, the above equation implies that

$$\frac{d}{dx_0} \mathcal{T}(x_0 = a - \epsilon) = \frac{d}{dx_0} \mathcal{T}(x_0 = a + \epsilon). \quad (\text{A3})$$

Writing it in terms of the notations $\mathcal{T}_{1,I}^L$ and $\mathcal{T}_{1,I}^H$ used in Section III A, implies Eq.(13). Since the derivative of the function MFPT is continuous, it follows that the MFPT

itself must also be continuous at $x_0 = a$. This yields Eqs. (13) and (14) of the main text.

The derivations of the connecting conditions, given in Eqs.(13) and (14), do not rely on any specific functional form of the potential $U(x_0)$. The only requirement for the validity of these conditions is that the potential $U(x_0)$ is continuous at $x_0 = a$, the position of the kink. Consequently, the same connecting conditions apply to the MFPT corresponding to the piecewise-harmonic potential defined in Eq.(18).

To compute the MFPT for the case of multiple intermediate barriers in a linear or harmonic potential, it is important to note that there are two connecting conditions at the position of each kink. In addition to these, we already have two boundary conditions: a reflecting boundary at $x_0 = 0$ and an absorbing boundary at $x_0 = 1$. Thus, for N kinks, we have a total of $2N + 2$ conditions that the MFPT function $\mathcal{T}(x_0)$ must satisfy. Furthermore, the presence of N kinks implies that the domain is divided into $N + 1$ segments or regions. The solution of the differential equation (Eq.(6)) within each region contains two undetermined integration constants. Therefore, across all $N + 1$ regions, there are $2(N + 1)$ integration constants in total. Since the number of independent conditions matches the number of unknown constants, all integration constants are uniquely determined. Consequently, the corresponding MFPT is fully specified.

Appendix B: Simulation Specification

To generate the numerical data presented in Fig.2, we simulated 10^5 independent trajectories of a Brownian particle. Each trajectory was initialized at $x = 0$ and evolved until the particle was absorbed at the boundary $x = 1$. The time evolution of the particle in each microscopic time scale dt can be written in terms of a discretized form of Langevin equation in 2 using Euler-Maruyama approximation such as

$$x(t + \Delta t) = x(t) - U'(x(t)) \Delta t + \sqrt{2D\Delta t} \mathcal{N}(0, 1), \quad (\text{B1})$$

where $\mathcal{N}(0, 1)$ denotes a Gaussian random variable with zero mean and unit variance. For the data corresponding to Fig.2(b), $dt = 10^{-5}$ was used, while for Fig.2(d), $dt =$

10^{-7} was employed to ensure numerical accuracy. In both cases, the barrier height was fixed at $\Delta U = 3$, and the position of the kink was set to $a = 0.3$.

- ¹R. Elber, D. E. Makarov, and H. Orland, *Molecular kinetics in condensed phases: theory, simulation, and analysis* (John Wiley & Sons, 2020).
- ²R. Metzler, S. Redner, and G. Oshanin, *First-passage phenomena and their applications*, Vol. 35 (World Scientific, 2014).
- ³S. Redner, *A guide to first-passage processes* (Cambridge university press, 2001).
- ⁴A. Szabo, K. Schulten, and Z. Schulten, "First passage time approach to diffusion controlled reactions," *The Journal of chemical physics* **72**, 4350–4357 (1980).
- ⁵A. J. Bray, S. N. Majumdar, and G. Schehr, "Persistence and first-passage properties in nonequilibrium systems," *Advances in Physics* **62**, 225–361 (2013).
- ⁶Y. Zhang and O. K. Dudko, "First-passage processes in the genome," *Annual review of biophysics* **45**, 117–134 (2016).
- ⁷A. M. Berezhkovskii and D. E. Makarov, "On distributions of barrier crossing times as observed in single-molecule studies of biomolecules," *Biophysical Reports* **1** (2021).
- ⁸H. A. Kramers, "Brownian motion in a field of force and the diffusion model of chemical reactions," *Physica* **7**, 284–304 (1940).
- ⁹C. Gardiner, *Stochastic methods*, Vol. 4 (Springer Berlin, 2009).
- ¹⁰P. Hänggi, P. Talkner, and M. Borkovec, "Reaction-rate theory: fifty years after kramers," *Reviews of modern physics* **62**, 251 (1990).
- ¹¹E. Woillez, Y. Zhao, Y. Kafri, V. Lecomte, and J. Tailleur, "Activated escape of a self-propelled particle from a metastable state," *Physical review letters* **122**, 258001 (2019).
- ¹²A. Militaru, M. Innerbichler, M. Frimmer, F. Tebbenjohanns, L. Novotny, and C. Dellago, "Escape dynamics of active particles in multistable potentials," *Nature Communications* **12**, 2446 (2021).
- ¹³L. Caprini, U. Marini Bettolo Marconi, A. Puglisi, and A. Vulpiani, "Active escape dynamics: The effect of persistence on barrier crossing," *The Journal of chemical physics* **150** (2019).
- ¹⁴L. Caprini, F. Cecconi, and U. Marini Bettolo Marconi, "Correlated escape of active particles across a potential barrier," *The Journal of Chemical Physics* **155** (2021).
- ¹⁵M. Asfaw and Y. Shiferaw, "Exploring the dynamics of dimer crossing over a kramers type potential," *The Journal of Chemical Physics* **136** (2012).
- ¹⁶E. Lyngdoh and W. Reenbohn, "Escape rate of a dimer under the influence of additive colored noise: Ornstein–uhlenbeck process," *Physica A: Statistical Mechanics and its Applications* **651**, 129975 (2024).
- ¹⁷R. Singh, "Kramers problem for a dimer: Effect of noise correlations," *Physical Review E* **95**, 042132 (2017).
- ¹⁸A. Barbier-Chebbah, O. Bénichou, R. Voituriez, and T. Guérin, "Long-term memory induced correction to arrhenius law," *arXiv preprint arXiv:2406.04720* (2024).
- ¹⁹V. Kumar, A. Pal, and O. Shpielberg, "Arrhenius law for interacting diffusive systems," *Physical Review E* **109**, L032101 (2024).
- ²⁰V. Kumar, A. Pal, and O. Shpielberg, "Emerging universality classes in thermally assisted activation of interacting diffusive systems: A perturbative hydrodynamic approach," *The Journal of Chemical Physics* **160** (2024).
- ²¹V. Kumar, A. Pal, and O. Shpielberg, "Inferring intermediate states by leveraging the many-body arrhenius law," *arXiv preprint arXiv:2412.18574* (2024).
- ²²J. Kappler, J. O. Daldrop, F. N. Brünig, M. D. Boehle, and R. R. Netz, "Memory-induced acceleration and slowdown of barrier crossing," *The Journal of Chemical Physics* **148** (2018).
- ²³A. Pal, V. Stojkoski, and T. Sandev, "Random resetting in search problems," in *Target Search Problems* (Springer, 2024) pp. 323–355.
- ²⁴S. Pal, D. Boyer, L. Dagdug, and A. Pal, "Channel-facilitated transport under resetting dynamics," *The Journal of Chemical Physics* **161** (2024).
- ²⁵R. Singh, R. Metzler, and T. Sandev, "Resetting dynamics in a confining potential," *Journal of Physics A: Mathematical and Theoretical* **53**, 505003 (2020).
- ²⁶S. Ahmad, I. Nayak, A. Bansal, A. Nandi, and D. Das, "First passage of a particle in a potential under stochastic resetting: A vanishing transition of optimal resetting rate," *Physical Review E* **99**, 022130 (2019).
- ²⁷K. Capala and B. Dybiec, "Optimization of escape kinetics by reflecting and resetting," *Chaos: An Interdisciplinary Journal of Nonlinear Science* **33** (2023).
- ²⁸S. Ray and S. Reuveni, "Diffusion with resetting in a logarithmic potential," *The Journal of chemical physics* **152** (2020).
- ²⁹T. Wellens, V. Shatokhin, and A. Buchleitner, "Stochastic resonance," *Reports on progress in physics* **67**, 45 (2003).
- ³⁰J. Kärger, S. Vasenkov, and S. M. Auerbach, "Diffusion in zeolites," in *Handbook of zeolite science and technology* (CRC Press, 2003) pp. 446–548.
- ³¹M. Gershow and J. A. Golovchenko, "Recapturing and trapping single molecules with a solid-state nanopore," *Nature nanotechnology* **2**, 775–779 (2007).
- ³²L. Dagdug, J. Peña, and I. Pompa-García, *Diffusion Under Confinement: A Journey Through Counterintuition*, Vol. 1 (Springer).
- ³³C. Wagner and T. Kiefhaber, "Intermediates can accelerate protein folding," *Proceedings of the National Academy of Sciences* **96**, 6716–6721 (1999).
- ³⁴V. V. Palyulin and R. Metzler, "How a finite potential barrier decreases the mean first-passage time," *Journal of Statistical Mechanics: Theory and Experiment* **2012**, L03001 (2012).
- ³⁵M. Chupéau, J. Gladrow, A. Chepelianskii, U. F. Keyser, and E. Trizac, "Optimizing brownian escape rates by potential shaping," *Proceedings of the National Academy of Sciences* **117**, 1383–1388 (2020).
- ³⁶R. Zwanzig, *Nonequilibrium statistical mechanics* (Oxford university press, 2001).
- ³⁷H. Risken and H. Risken, *Fokker-planck equation* (Springer, 1996).
- ³⁸D. G. Grier and Y. Roichman, "Holographic optical trapping," *Applied optics* **45**, 880–887 (2006).
- ³⁹Y. Roichman, V. Wong, and D. G. Grier, "Colloidal transport through optical tweezer arrays," *Physical Review E—Statistical, Nonlinear, and Soft Matter Physics* **75**, 011407 (2007).
- ⁴⁰B. R. Ferrer and J. R. Gomez-Solano, "Experimental measurement of mean transition path velocities of colloidal particles surmounting energy barriers," *New Journal of Physics* **26**, 123022 (2024).
- ⁴¹A. L. Thorneywork, J. Gladrow, Y. Qing, M. Rico-Pasto, F. Rittort, H. Bayley, A. B. Kolomeisky, and U. F. Keyser, "Direct detection of molecular intermediates from first-passage times," *Science advances* **6**, eaaz4642 (2020).
- ⁴²M. Bekele, G. Ananthakrishna, and N. Kumar, "Optimal barrier subdivision for kramers' escape rate," *Pramana* **46**, 403–410 (1996).